THE FALLACY OF DRIFTING SNOW

Edgar L Andreas*
NorthWest Research Associates, Inc.
Lebanon, New Hampshire

1. INTRODUCTION

Once Owen (1964) proposed that the height of the saltation layer over a mobile surface, like sand or snow, sets the aerodynamic roughness length (z_0), many snow scientists embraced this parameterization. Briefly, Owen's argument requires

$$z_0 = \alpha \frac{u_*^2}{g} , \qquad (1.1)$$

where u_* is the friction velocity, g is the acceleration of gravity, and α is a constant.

Earlier, Charnock (1955) had used dimensional analysis and measurements of the vertical wind speed profile over a natural water body to obtain the same result empirically. When (1.1) is applied to the aerodynamic roughness of water surfaces, it is referred to as the Charnock relation.

Chamberlain (1983) subsequently argued that (1.1), with a single α value of about 0.016, works equally well over sand, snow, and the sea (cf. Wieringa 1993). Many flux parameterizations over both the ocean and snow-covered terrain therefore use (1.1) to parameterize z_0.

Values of the constant α obtained over the ocean generally fall in the range 0.01–0.02 (e.g., Smith 1988; Fairall et al. 1996; Johnson et al. 1998; Bonekamp et al. 2002). Some values of α measured over surfaces with drifting snow are also in this range and therefore seem to support Chamberlain's (1983) synthesis. For example, Kind (1976) found $\alpha = 0.010$, and Tabler (1980) suggested $\alpha = 0.013$. But, in general, the value of α over snow-covered surfaces seems much more variable than over the ocean. Pomeroy and Gray (1990) measured $\alpha = 0.06$ for snow-covered ground; König (1985) reported $\alpha = 0.006$ for an Antarctic ice shelf; Andreas and Claffey (1995) obtained $\alpha = 0.097$ over Antarctic sea ice; and Liston and Sturm (1998) used $\alpha = 0.6$ in their model for drifting snow over complex terrain (although I suspect that this value may be a typographical error that is 10 times too large). Finally, Schmidt's (1986) data, collected over a frozen, snow-covered lake in Wyoming, did not fit the dependence suggested in (1.1).

Because of the variety of α values obtained over saltating surfaces, Raupach (1991) and Andreas and Claffey (1995) suggested that (1.1) is not strictly appropriate for solid surfaces with mobile roughness elements on top of them. Such surfaces are not like the ocean, whose surface is perfectly planar in the absence of wind. Rather, for snow-covered surfaces, the underlying topography likely dictates the general range of α; it is thus not a universal constant. Andreas (2011) goes into more detail on how z_0 parameterizations over snow-covered surfaces need to be site specific.

Another issue arises, however, in validating (1.1) with data. As I will explain shortly, most experimental evaluations of z_0 on the left side of (1.1) require the same friction velocity, u_*, that appears on the right side of (1.1). Consequently, plots of z_0 versus u_* have built-in correlation—termed fictitious correlation here—that naturally causes z_0 to increase with u_*, as (1.1) predicts. I believe that this fictitious correlation—not any real physics—explains why (1.1) has endured.

In this paper, I treat this issue of fictitious correlation in parameterizations of z_0 over snow-covered surfaces. I first explain mathematically how typical data analyses automatically require measured z_0 values to increase with measured u_* values. I next demonstrate this effect with two large datasets collected over snow-covered sea ice: one from the Arctic (from SHEBA, the experiment to study the Surface Heat Budget of the Arctic Ocean), and one from the Antarctic (data from Ice Station Weddell). Finally, I demonstrate the proper way to evaluate how or whether z_0 depends on u_*. When z_0 is evaluated from measured u_* values but plotted against the u_* values obtained from a bulk flux algorithm (a processes that minimizes fictitious correlation), z_0

* *Corresponding author address:* Dr. Edgar L Andreas, NorthWest Research Associates, Inc. (Seattle Division), 25 Eagle Ridge, Lebanon, NH 03766-1900; e-mail: eandreas@nwra.com.

is independent of this bulk u_* in the drifting snow region ($u_* \geq 0.3$ m s^{-1}), contrary to what (1.1) predicts. I thus conclude that (1.1) is a fallacious result made plausible by flawed analyses.

2. BULK FLUX ALGORITHM

A key use for parameterizations of z_0 is in bulk turbulent flux algorithms. Such algorithms (cf. Fairall et al., 1996, 2003) are used for estimating the turbulent surface fluxes of momentum (τ, also called the surface stress) and sensible (H_s) and latent (H_L) heat in analyses and models. In fact, almost all weather and climate models determine the surface fluxes from such bulk flux algorithms (Wyngaard 2010).

One of the goals of SHEBA was to develop bulk flux algorithms for winter and summer sea ice (Andreas et al. 1999; Uttal et al. 2002). I will invoke the winter algorithm later in this paper. Andreas et al. (2010a, 2010b) give the full details of both SHEBA bulk turbulent flux algorithms. Hence, here I will describe only the basic equations.

The main equations are based on Monin-Obukhov similarity theory and take the forms (e.g., Garratt, 1992, p. 52ff.)

$$\tau \equiv \rho u_*^2 = \rho C_{Dr} S_r^2 , \qquad (2.1a)$$

$$H_s = \rho c_p C_{Hr} S_r (\Theta_s - \Theta_r) , \qquad (2.1b)$$

$$H_L = \rho L_s C_{Er} S_r (Q_s - Q_r) . \qquad (2.1c)$$

Here, ρ is the air density; c_p is the specific heat of air at constant pressure; L_s is the latent heat of sublimation; S_r is an effective wind speed at reference height r; Θ_r and Q_r are the potential temperature and specific humidity, respectively, at height r; and Θ_s and Q_s are the temperature and specific humidity at the surface. Because the surface is snow or ice, we evaluate Q_s as the saturation value at temperature Θ_s. Equation (2.1a) also defines the friction velocity, u_*.

The essence of any bulk flux algorithm is how it evaluates the transfer coefficients for momentum, sensible heat, and latent heat appropriate for reference height r: respectively, C_{Dr}, C_{Hr}, and C_{Er} in (2.1). These derive from Monin-Obukhov similarity theory and formally are

$$C_{Dr} = \frac{k^2}{\left[\ln(r/z_0) - \psi_m(r/L)\right]^2} , \qquad (2.2a)$$

$$C_{Hr} = \frac{k C_{Dr}^{1/2}}{\left[\ln(r/z_T) - \psi_h(r/L)\right]} , \qquad (2.2b)$$

$$C_{Er} = \frac{k C_{Dr}^{1/2}}{\left[\ln(r/z_Q) - \psi_h(r/L)\right]} . \qquad (2.2c)$$

In these equations, k (= 0.40) is the von Kármán constant, and ψ_m and ψ_h are empirical functions of the Obukhov length

$$L = -\frac{\overline{\Theta}}{k g}\left(\frac{u_*^3}{\left(\frac{H_s}{\rho c_p}\right) + \frac{0.61\overline{\Theta}}{1+0.61\overline{Q}}\left(\frac{H_L}{\rho L_s}\right)}\right) . \qquad (2.3)$$

Here, g is, again, the acceleration of gravity, and $\overline{\Theta}$ and $\overline{Q}$ are surface-layer averages of the air temperature and specific humidity.

Andreas et al. (2010a, 2010b; cf. Fairall et al. 1996, 2003; Andreas et al. 2008) explain that S_r in (2.1) is not just the measured or modeled wind speed but also includes a parameterization for gustiness. Andreas et al. also explain how the SHEBA algorithms parameterize z_0, z_T, z_Q, ψ_m, and ψ_h. As with most bulk flux algorithms, (2.1) and (2.2) are coupled through the Obukhov length, (2.3), and therefore must be solved iteratively.

3. DATA

Ice Station Weddell drifted from early February through early June 1992 in the western Weddell Sea, paralleling the track of Shackleton's *Endurance*. Andreas and Claffey (1995) and Andreas et al. (2004, 2005) give full details of the mean and turbulence data collected on Ice Station Weddell.

Briefly, the turbulence data relevant to this paper came from a sonic anemometer/thermometer and a Lyman-alpha hygrometer mounted on a tower at a height of 4.65 m and sampled at 10 Hz. The turbulent fluxes were averaged hourly and calculated as covariances: that is,

$$\tau = -\rho \overline{uw} , \qquad (3.1a)$$

$$H_s = \rho c_p \overline{w\theta} \ , \qquad (3.1b)$$

$$H_L = \rho L_s \overline{wq} \ . \qquad (3.1c)$$

Here, u, w, θ, and q are turbulent fluctuations in longitudinal velocity, vertical velocity, temperature, and specific humidity; the overbar indicates an hour of averaging.

We did the usual coordinate rotations to align $\overline{uw}$ with the mean wind and made a Webb correction to H_L. The turbulence measurements ran continuously from late February through late May 1992; we exclude data, though, when the air flow was disturbed by structures on Ice Station Weddell. The surface at Ice Station Weddell was compact, second-year sea ice with a snow cover typically 0.4–0.5 m deep.

The SHEBA ice camp drifted in the Beaufort Gyre from early October 1997 until early October 1998. Our Atmospheric Surface Flux Group maintained a site in the main camp centered on a 20-m tower that was instrumented at five levels with sonic anemometer/thermometers. We also maintained three to four remote sites instrumented with Flux-PAM stations (Militzer et al. 1995; Horst et al. 1997). I use data from the Flux-PAM site called Baltimore here as a representative of the other SHEBA remote sites and because its one-level flux measurements are comparable to the measurements on Ice Station Weddell. Persson et al. (2002), Grachev et al. (2005, 2007), Brunke et al. (2006), and Andreas et al. (2006, 2010a, 2010b) describe the SHEBA measurements in detail.

As brief background, the Flux-PAM stations measured τ and H_s hourly with a sonic anemometer/thermometer at a height that ranged from 2.3 to 3.5 m above the surface. Processing was as eddy covariances, as on Ice Station Weddell. There were no latent heat flux measurements at the PAM sites.

Andreas et al. (2010a, 2010b; cf. Brunke et al. 2006) divided the SHEBA year into just two aerodynamic seasons, winter and summer, on the basis of ice conditions. In "winter," the sea ice was compact and continuously snow-covered, and the snow was dry enough to drift and blow. In "summer," the snow became too wet and sticky to drift and eventually disappeared entirely at the SHEBA camp to expose bare sea ice. In this paper, I focus on the SHEBA winter data because only this period includes episodes of drifting snow, and the data should also be comparable to the data from the entire Ice Station Weddell deployment. During SHEBA, winter ran from the beginning of the measurements in late October 1997 through 14 May 1998. It resumed on 15 September 1998 and continued through the end of September, when we began closing the SHEBA camp.

From the SHEBA and Ice Station Weddell data, I evaluated z_0 from (2.1a) and (2.2a) as

$$z_0 = r \exp\left\{-\left[k C_{Dr}^{-1/2} + \psi_m(r/L)\right]\right\}, \qquad (3.2)$$

where z_0 and r are in meters. All quantities on the right here were measured or otherwise known. In particular, for ψ_m, I used the function from Paulson (1970) in unstable stratification and the function from Grachev et al. (2007) in stable stratification. I screened the resulting hourly values and discounted four Ice Station Weddell cases and 153 Baltimore cases for which $z_0 \geq 0.1$ m. Computed values of z_0 this large over compact, snow-covered ice are obviously erroneous (e.g., Banke et al. 1980; Overland 1985; Guest and Davidson 1991; Andreas 1995). This screening retained 866 Ice Station Weddell cases and 1470 Baltimore cases for use here.

After finding z_0 from (3.2), I could also calculate the drag coefficient for neutral stability at a standard reference height of 10 m from (2.2a) as

$$C_{DN10} = \left[\frac{k}{\ln(10/z_0)}\right]^2 . \qquad (3.3)$$

This and z_0 are interchangeable quantities for characterizing the aerodynamic properties of a surface.

4. FICTITIOUS CORRELATION IN z_0–u_* PLOTS

Equation (1.1) is a standard expression for parameterizing the roughness length z_0 over any snow-covered surface (e.g., Radok 1968; Kind 1976; Tabler 1980; Male 1980; Pomeroy and Gray 1990; Pomeroy et al. 1993; Déry and Taylor 1996; Liston and Sturm 1998; Andreas et al. 2005). For the purpose of trying to better understand how to parameterize z_0 and, therefore, u_* for snow-covered sea ice (cf. Andreas 2011), I would like to revisit (1.1). I believe that most experimental validations of it suffered from fictitious correlation (e.g., Andreas et al. 2010b).

Figure 1 shows what typical plots that attempt to relate z_0 to u_* look like. The data come from both Ice Station Weddell and the SHEBA Flux-

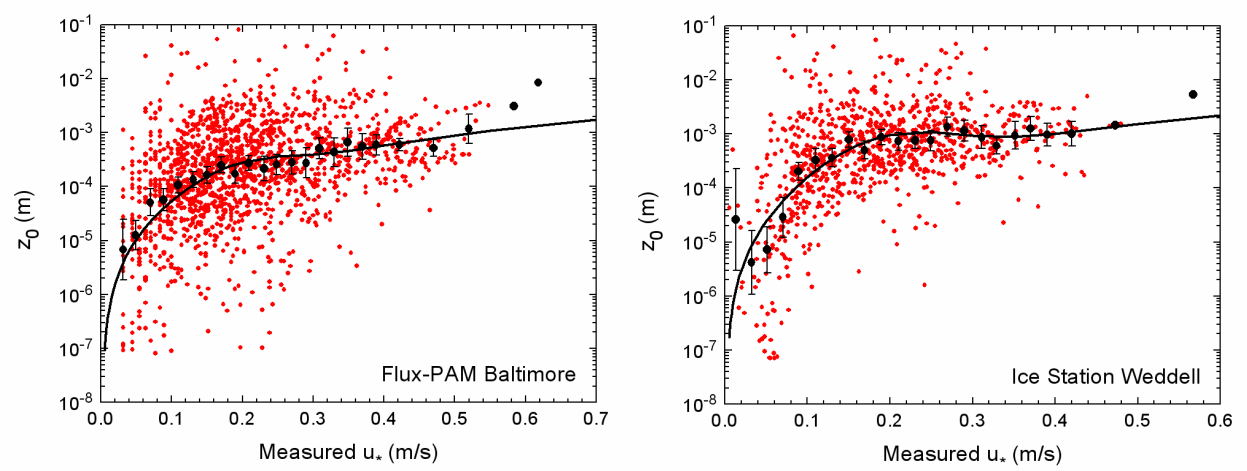

FIG. 1. Hourly measurements of the aerodynamic roughness length z_0 from (3.2) made over winter sea ice (red circles) are plotted against measured values of the friction velocity, u_*. The data come from the SHEBA Flux-PAM site named Baltimore and from Ice Station Weddell. The black circles are geometric mean values of z_0 in u_* bins that are mostly 2 cm s^{-1} wide; the error bars show ±2 times the standard deviation in the geometric mean. Equation (4.1) gives the expression for the solid curves.

PAM site called Baltimore. The z_0 values clearly tend to increase throughout the u_* range; the increase is most pronounced for small u_* in the region well below the snow saltation threshold (Figure 2). Both figures also show z_0 increasing with u_* above the saltation threshold of about $u_* = 0.30\,m\,s^{-1}$.

Taking guidance from Andreas et al. (2005), I fitted similar functions to both panels in Figure 1:

$$z_0 = \frac{\alpha u_*^2}{g}\left\{F\exp\left[-\left(\frac{u_* - 0.18}{0.10}\right)^2\right] + 1\right\} . \quad (4.1)$$

Here, z_0 is in meters, u_* is in m s^{-1}, and g is in m s^{-2}. In the Baltimore panel in Figure 1, $\alpha = 0.035$ and $F = 1$; in the Ice Station Weddell panel, $\alpha = 0.060$ and $F = 3$.

Both panels in Figure 1 probably suffer from fictitious correlation, however, because I evaluated z_0 from (3.2) in the form

$$z_0 = r\exp\left\{-\left[\frac{kS_r}{u_*} + \psi_m(r/L)\right]\right\} . \quad (4.2)$$

That is, in Figure 1, the measured u_* appears prominently in both the dependent and independent variables. (Remember, L also includes u_*.)

In the literature, the data for z_0–u_* plots often come from measurements of the wind speed profile $U(z)$, where z is the measurement height. Because the wind speed measured in the atmospheric surface layer is presumed to obey Monin-Obukhov similarity, its profile is represented as

$$U(z) = \frac{u_*}{k}\left[\ln(z/z_0) - \psi_m(z/L)\right] . \quad (4.3)$$

The stability correction ψ_m here makes using (4.3) to analyze data difficult unless we also have simultaneous profile measurements of potential temperature and specific humidity and can thereby iteratively solve the three profile equations for the Obukhov length. In the absence of these extra profiles, most determinations of u_* and z_0 from profile measurements require near-neutral stratification, when (4.3) simplifies to

$$U(z) = \frac{u_*}{k}\ln(z) - \frac{u_*}{k}\ln(z_0) . \quad (4.4)$$

In such neutral stratification, plots of $U(z)$ versus $\ln(z)$ can be fit with a straight line such that the slope is u_*/k and the intercept (I) is $-(u_*/k)\ln(z_0)$. This analysis similarly produces

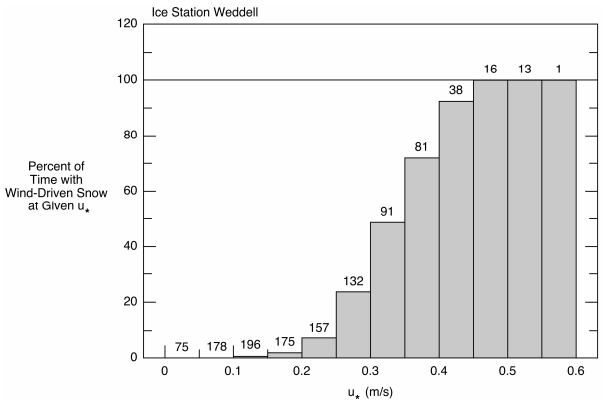

FIG. 2. Observations on Ice Station Weddell of the occurrence of drifting and blowing snow as a function of the measured friction velocity, u_*. The chart shows the percentage of observations within a u_* bin for which we observed drifting and blowing snow. The number above each bar is a count of the observation periods for which u_* was in that interval. (Observation frequency varied but was typically eight times per day.) Clearly, the threshold for drifting snow on Ice Station Weddell was in the u_* range 0.25–0.35 m s^{-1}.

fictitious correlation between z_0 and u_* because here z_0 is calculated as

$$z_0 = \exp\left(-\frac{k I}{u_*}\right) . \qquad (4.5)$$

But for any reference height r, (4.4) provides the relation

$$I = U_r - \frac{u_*}{k}\ln(r) , \qquad (4.6)$$

where U_r is the wind speed at height r. Consequently, with (4.6) inserted for I, (4.5) becomes

$$z_0 = r\exp\left(-\frac{k U_r}{u_*}\right) , \qquad (4.7)$$

which is similar to the expression that we get from eddy-covariance measurements, (4.2). That is, here too, the measured u_* is embedded in z_0.

To see what effect this shared u_* has on analyses of z_0 versus u_*, I rewrite (4.2) as

$$\ln(z_0) = \ln(r) - \left[\frac{k S_r}{u_*} + \psi_m(r/L)\right] \qquad (4.8)$$

because Figure 1 shows plots of $\ln(z_0)$ versus u_*. I now take the differential of (4.8) but ignore the ψ_m term, which is usually minor [cf. (4.7)]:

$$d\ln(z_0) = \frac{dr}{r} + \frac{k S_r}{u_*}\left(\frac{du_*}{u_*} - \frac{dS_r}{S_r}\right) . \qquad (4.9)$$

I interpret $d\ln(z_0)$, dr, du_*, and dS_r as errors in individual measurements (i.e., hourly values) of $\ln(z_0)$, r, u_*, and S_r; the r, u_*, and S_r in (4.9) are hourly or other long-term averages. Because r does not change with each measurement, the dr/r term in (4.9) could cause a bias error in $\ln(z_0)$ but probably not a random error. The du_*/u_* and dS_r/S_r terms, on the other hand, lead to random errors in $\ln(z_0)$. From Table 1 in Andreas et al. (2010b), we see that du_*/u_* is typically 0.1, while dS_r/S_r is generally much smaller—often less than 0.01.

Because kS_r/u_* is always positive, the upshot of (4.9) is that errors in $\ln(z_0)$ are positively correlated with errors in u_*. When u_* is measured erroneously large, $\ln(z_0)$ is evaluated erroneously large. When u_* is measured erroneously small, $\ln(z_0)$ is evaluated erroneously small. Plots of $\ln(z_0)$ versus measured u_*, as in Figure 1, thus naturally tend to show $\ln(z_0)$ increasing with u_* because of the shared u_*—an effect that I call fictitious correlation (e.g., Andreas and Hicks, 2001; Andreas, 2002, 2009; Andreas et al., 2006).

To mitigate the misleading effects of such fictitious correlation in scatter plots such as those in Figure 1, Andreas et al. (2006, 2010b) suggested using, in the independent variable, quantities calculated from a bulk flux algorithm instead of measured quantities. In other words, as the independent variable in Figure 1, replace the measured u_* with the u_* from a bulk flux algorithm. In fact, this is the proper approach for developing and validating bulk flux algorithms. Because of the coupling among the equations in these algorithms, the goal is to iteratively obtain an accurate estimate of z_0, for example, that is associated with the bulk estimate of u_*.

Figure 3 shows the difference that this approach makes in interpreting the behavior of z_0.

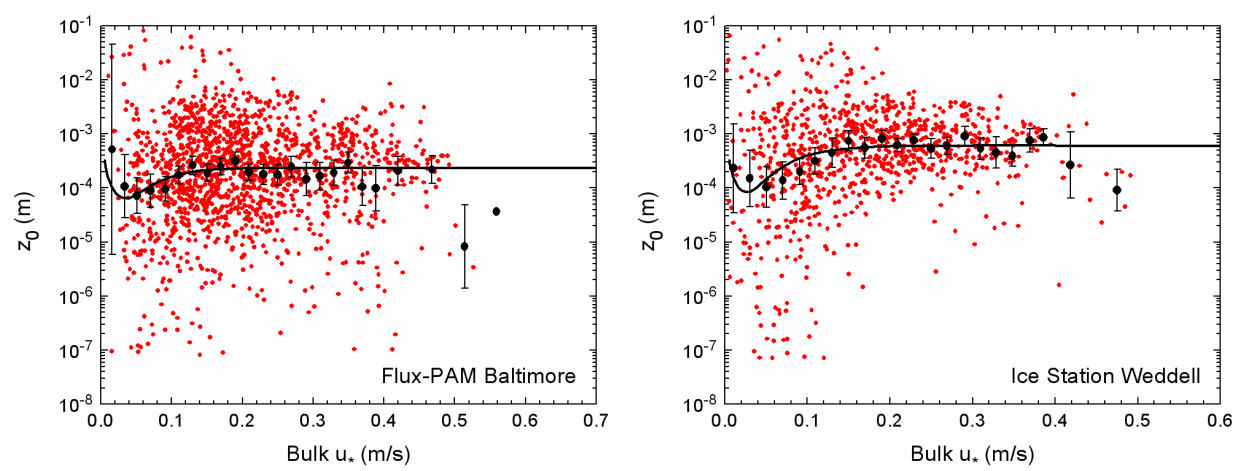

FIG. 3 The same z_0 values as in Figure 1. Here, though, the independent variable is the u_* value from a bulk flux algorithm, $u_{*,B}$. The curves in the two panels are (4.10), with $B=2.3\times10^{-4}$ for the Baltimore panel and with $B=6.0\times10^{-4}$ for the Ice Station Weddell panel.

The two panels show the same z_0 measurements as in Figure 1; but now the independent variable is an estimate of u_* from a bulk flux algorithm (denoted $u_{*,B}$). Neither panel exhibits the dramatic decrease in z_0 with decreasing u_* that we saw in Figure 1. And when u_* is above the range influenced by aerodynamically smooth flow (i.e., $u_{*,B}>0.2\,m s^{-1}$), z_0 is constant: That is, it does not increase with friction velocity as it did in Figure 1.

The increase with increasing u_* that z_0 exhibits in Figure 1 is consequently an artifact of the shared measurements of u_*: It is fictitious correlation. For u_* values below 0.6 m s^{-1}, neither the SHEBA nor Ice Station Weddell data show any evidence that blowing snow causes z_0 to increase. Four other independent datasets from SHEBA (see Figure 2 in Andreas et al. 2010b) demonstrate this same result.

The curves in the two panels in Figure 3 have the form

$$z_0 = 0.135\frac{\nu}{u_{*,B}} + B\tanh^3\left(13\,u_{*,B}\right), \quad (4.10)$$

where z_0 is in meters, $u_{*,B}$ is in m s^{-1}, and ν is the kinematic viscosity of air in m^2 s^{-1}. Equation (4.10) with $B=2.3\times10^{-4}$ is from the SHEBA bulk flux algorithm (Andreas et al., 2010b) and is plotted in the Baltimore panel in Figure 3. In the Ice Station Weddell panel, (4.10) with $B=6.0\times10^{-4}$ fits the z_0 data better. I used (4.10) with the respective B values in the bulk flux algorithm with which I computed $u_{*,B}$ in the Baltimore and Ice Station Weddell panels in Figure 3.

The most conspicuous differences between Figures 1 and 3 is in the behavior of z_0 for small u_*. In Figure 1, z_0 gets smaller as the measured u_* gets smaller. Figure 3, in contrast, suggests that z_0 obeys aerodynamically smooth scaling for small u_* when plotted against the bulk u_*: z_0 gets larger as u_* gets smaller for small u_*. The first term on the right side of (4.10) represents this behavior. In effect, the fictitious correlation completely obscures the known theoretical and empirical behavior of z_0 for small u_*.

In summary, from the results in this section, I conclude that the idea that the roughness length z_0 for drifting snow increases with u_*^2 is a fallacy that has persisted because of flawed analyses. Scatter plots of measured z_0 versus measured u_* (e.g., Figure 1) suffer from fictitious correlation because the measured u_* is also required for calculating z_0. Hence, errors in u_* are translated into corresponding errors in z_0. Plots of measured z_0 against a bulk flux estimate of u_*, on the other hand (as in Figure 3), mitigate the fictitious correlation and show no increase in z_0 with $u_{*,B}$ in the drifting snow regime, at least up to $u_{*,B}$ of 0.6 m s^{-1}.

In effect, this analysis demonstrates that snow-covered sea ice—and probably any snow-covered surface—is not a mobile surface in the same sense that the ocean is; its roughness length does not increase with friction velocity for the wind speeds I have observed.

5. CONCLUSIONS

The roughness length, z_0, over snow-covered surfaces is often presumed to scale with the friction velocity, u_*. Measurements of z_0 are, thus, typically plotted against measurements of u_* and exhibit a Charnock-like behavior, (1.1). The implication is that snow behaves as a mobile surface such that z_0 increases with the square of u_* when snow begins drifting at a threshold u_* value of about 0.3 m s^{-1}.

Data from both SHEBA and Ice Station Weddell, however, suggest that plots showing z_0 to increase with u_* suffer from fictitious correlation because the u_* measurements are necessary for calculating z_0 (see Figure 1). In other words, the dependent and independent variables include some of the same measurements and, thus, have built-in correlation that obscures the physics.

The proper way to compare z_0 with u_* and the proper way to develop a bulk flux algorithm is to plot the z_0 measurements against the u_* values estimated with a bulk algorithm or against another independently obtained u_*. In such plots (e.g., Figure 3), z_0 is independent of the bulk u_* in the drifting snow region (i.e., $u_{*B} \geq 0.3\, m s^{-1}$). My conclusion is, therefore, that the idea that drifting snow causes z_0 to increase with friction velocity is a fallacy perpetuated by analyses that suffered from fictitious correlation.

6. ACKNOWLEDGMENTS

I would like to thank my colleagues in the SHEBA Atmospheric Surface Flux Group for help collecting, processing, and understanding the SHEBA data: Chris Fairall, Andrey Grachev, Peter Guest, Tom Horst, Rachel Jordan, and Ola Persson. I would also like to thank the other members of the meteorology team on Ice Station Weddell for help collecting the data there: Kerry Claffey, Boris Ivanov, and Aleksandr Makshtas. The U.S. National Science Foundation (NSF) supported this work with awards 06-11942 and 10-19322. NSF also supported my programs on Ice Station Weddell and at SHEBA with previous awards.

7. REFERENCES

Andreas, E. L, 1995: Air-ice drag coefficients in the western Weddell Sea: 2. A model based on form drag and drifting snow. *J. Geophys. Res.*, **100** (C3), 4833–4843.

____, 2002: Parameterizing scalar transfer over snow and ice: A review. *J. Hydrometeor.*, **3**, 417–432.

____, 2009: Relating the drag coefficient and the roughness length over the sea to the wavelength of the peak waves. *J. Phys. Oceanogr.*, **39**, 3011–3020.

____, 2011: Relationship between the aerodynamic and physical roughness of winter sea ice. *Quart. J. Roy. Meteor. Soc.*, submitted.

____, and K. J. Claffey, 1995: Air-ice drag coefficients in the western Weddell Sea: 1. Values deduced from profile measurements. *J. Geophys. Res.*, **100** (C3), 4821–4831.

____, and B. B. Hicks, 2002: Comments on "Critical test of the validity of Monin-Obukhov similarity during convective conditions." *J. Atmos. Sci.*, **59**, 2605–2607.

____, C. W. Fairall, P. S. Guest, and P. O. G. Persson, 1999: An overview of the SHEBA atmospheric surface flux program. Preprints, *Fifth Conf. on Polar Meteorology and Oceanography*, Dallas, TX, Amer. Meteor. Soc., 411–416.

____, R. E. Jordan, and A. P. Makshtas, 2004: Simulations of snow, ice, and near-surface atmospheric processes on Ice Station Weddell. *J. Hydrometeor.*, **5**, 611–624.

____, ____, and ____, 2005. Parameterizing turbulent exchange over sea ice: The Ice Station Weddell results. *Bound.-Layer Meteor.*, **114**, 439–460.

____, K. J. Claffey, R. E. Jordan, C. W. Fairall, P. S. Guest, P. O. G. Persson, and A. A. Grachev, 2006: Evaluations of the von Kármán constant in the atmospheric surface layer. *J. Fluid Mech.*, **559**, 117–149.

____, P. O. G. Persson, and J. E. Hare, 2008: A bulk turbulent air-sea flux algorithm for high-wind, spray conditions. *J. Phys. Oceanogr.*, **38**, 1581–1596.

____, T. W. Horst, A. A. Grachev, P. O. G. Persson, C. W. Fairall, P. S. Guest, and R. E. Jordan, 2010a: Parameterising turbulent exchange over summer sea ice and the

marginal ice zone. *Quart. J. Roy. Meteor. Soc.*, **136**, 927–943.

____, P. O. G. Persson, R. E. Jordan, T. W. Horst, P. S. Guest, A. A. Grachev, and C. W. Fairall, 2010b: Parameterizing turbulent exchange over sea ice in winter. *J. Hydrometeor.*, **11**, 87–104.

Banke, E. G., S. D. Smith, and R. J. Anderson, 1980: Drag coefficients at AIDJEX from sonic anemometer measurements. *Sea Ice Processes and Models*, R. S. Pritchard, Ed., University of Washington Press, 430–442.

Bonekamp, H., G. J. Komen, A. Sterl, P. A. E. M. Janssen, P. K. Taylor, and M. J. Yelland, 2002: Statistical comparisons of observed and ECMWF modeled open ocean surface drag. *J. Phys. Oceanogr.*, **32**, 1010–1027.

Brunke, M. A., M. Zhou, X. Zeng, and E. L Andreas, 2006: An intercomparison of bulk aerodynamic algorithms used over sea ice with data from the Surface Heat Budget for the Arctic Ocean (SHEBA) experiment. *J. Geophys. Res.*, **111**, C09001, doi: 10.1029/2005JC002907.

Chamberlain, A. C., 1983: Roughness length of sea, sand, and snow. *Bound.-Layer Meteor.*, **25**, 405–409.

Charnock, H., 1955: Wind stress on a water surface. *Quart. J. Roy. Meteor. Soc.*, **81**, 639.

Déry, S. J., and P. A. Taylor, 1996: Some aspects of the interaction of blowing snow with the atmospheric boundary layer. *Hydrol. Proc.*, **10**, 1345–1358.

Fairall, C. W., E. F. Bradley, D. P. Rogers, J. B. Edson, and G. S. Young, 1996: Bulk parameterization of air-sea fluxes for Tropical Ocean-Global Atmosphere Coupled-Ocean Atmosphere Response Experiment. *J. Geophys. Res.*, **101** (C2), 3747–3764.

____, ____, J. E. Hare, A. A. Grachev, and J. B. Edson, 2003: Bulk parameterization of air-sea fluxes: Updates and verification for the COARE algorithm. *J. Climate*, **16**, 571–591.

Garratt, J. R., 1992: *The Atmospheric Boundary Layer*. Cambridge University Press, 316 pp.

Grachev, A. A., C. W. Fairall, P. O. G. Persson, E. L Andreas, and P. S. Guest, 2005: Stable boundary-layer scaling regimes: The SHEBA data. *Bound.-Layer Meteor.*, **116**, 201–235.

____, E. L Andreas, C. W. Fairall, P. S. Guest, and P. O. G. Persson, 2007: SHEBA flux-profile relationships in the stable atmospheric boundary layer. *Bound.-Layer Meteor.*, **124**, 315–333.

Guest, P. S., and K. L. Davidson, 1991: The aerodynamic roughness of different types of sea ice. *J. Geophys. Res.*, **96**, 4709–4721.

Horst, T. W., S. P. Oncley, and S. R. Semmer, 1997: Measurement of water vapor fluxes using capacitance RH sensors and cospectral similarity. Preprints, *12th Symp. on Boundary Layers and Turbulence*, Vancouver, BC, Amer. Meteor. Soc., 360–361.

Johnson, H. K., J. Højstrup, H. J. Vested, and S. E. Larsen, 1998: On the dependence of sea surface roughness on wind waves. *J. Phys. Oceanogr.*, **28**, 1702–1716.

Kind, R. J., 1976: A critical examination of the requirements for model simulation of wind-induced erosion/deposition phenomena such as drifting snow. *Atmos. Environ.*, **10**, 219–227.

König, G., 1985: Roughness length of an Antarctic ice sheet. *Polarforschung*, **55**, 27–32.

Liston, G. E., and M. Sturm, 1998: A snow-transport model for complex terrain. *J. Glaciol.*, **44**, 498–516.

Male, D. H., 1980: The seasonal snow cover. *Dynamics of Snow and Ice Masses*, S. C. Colbeck, Ed., Academic Press, 305–395.

Militzer, J. M., M. C. Michaelis, S. R. Semmer, K. S. Norris, T. W. Horst, S. P. Oncley, A. C. Delany, and F. V. Brock, 1995: Development of the prototype PAM III/Flux-PAM surface meteorological station. Preprints, *Ninth Symp. on Meteorological Observations and Instrumentation*, Charlotte, NC, Amer. Meteor. Soc., 490–494.

Overland, J. E., 1985: Atmospheric boundary layer structure and drag coefficients over sea ice. *J. Geophys. Res.*, **90** (C5), 9029–9049.

Owen, P. R., 1964: Saltation of uniform grains in air. *J. Fluid Mech.*, **20**, 225–242.

Paulson, C. A., 1970: The mathematical representation of wind speed and temperature profiles in the unstable atmospheric surface layer. *J. Appl. Meteor.*, **9**, 857–861.

Persson, P. O. G., C. W. Fairall, E. L Andreas, P. S. Guest, and D. K. Perovich, 2002: Measurements near the Atmospheric Surface Flux Group tower at SHEBA: Near-surface conditions and surface energy budget. *J. Geophys. Res.*, **107**, 8045, doi: 10.1029/2000JC000705.

Pomeroy, J. W., and D. M. Gray, 1990: Saltation of snow. *Water Resour. Res.*, **26**, 1583–1594.

____, ____, and P. G. Landine, 1993: The prairie blowing snow model: Characteristics, validation, operation. *J. Hydrol.*, **144**, 165–192.

Radok, U., 1968: Deposition and erosion of snow by the wind. Res. Rep. 230, U.S. Army Cold Regions Research and Engineering Laboratory, Hanover, NH, 23 pp.

Raupach, M. R., 1991: Saltation layers, vegetation canopies and roughness lengths. *Acta Mech.* (Suppl.), **1**, 83–96.

Schmidt, R. A., 1986: Transport rate of drifting snow and the mean wind speed profile. *Bound.-Layer Meteor.*, **34**, 213–241.

Smith, S. D., 1988: Coefficients for sea surface wind stress, heat flux, and wind profiles as a function of wind speed and temperature. *J. Geophys. Res.*, **93** (C12), 15,467–15,472.

Tabler, R. D., 1980: Self-similarity of wind profiles in blowing snow allows outdoor modeling. *J. Glaciol.*, **26**, 421–434.

Uttal, T., and 27 others, 2002: Surface Heat Budget of the Arctic Ocean. *Bull. Amer. Meteor. Soc.*, **83**, 255–275.

Wieringa, J., 1993: Representative roughness parameters for homogeneous terrain. *Bound.-Layer Meteor.*, **63**, 323–363.

Wyngaard, J. C., 2010: *Turbulence in the Atmosphere*. Cambridge University Press, 393 pp.